

# Statistics of Dark Matter Substructure: II. Comparison of Model with Simulation Results

Frank C. van den Bosch<sup>1\*</sup>, Fangzhou Jiang<sup>1</sup>

<sup>1</sup>*Department of Astronomy, Yale University, PO Box 208101, New Haven, CT 06520-8101*

## ABSTRACT

We compare subhalo mass and velocity functions obtained from different simulations with different subhalo finders among each other, and with predictions from the new semi-analytical model of Jiang & van den Bosch (2014). We find that subhalo mass functions (SHMFs) obtained using different subhalo finders agree with each other at the level of  $\sim 20$  percent, but only at the low mass end. At the massive end, subhalo finders that identify subhaloes based purely on density in configuration space dramatically underpredict the subhalo abundances by more than an order of magnitude. These problems are much less severe for subhalo velocity functions (SHVFs), indicating that they arise from issues related to assigning masses to the subhaloes, rather than from detecting them. Overall the predictions from the semi-analytical model are in excellent agreement with simulation results obtained using the more advanced subhalo finders that use information in six dimensional phase-space. In particular, the model accurately reproduces the slope and host-mass-dependent normalization of both the subhalo mass and velocity functions. We find that the SHMFs and SHVFs have power-law slopes of 0.82 and 2.6, respectively, significantly shallower than what has been claimed in several studies in the literature.

**Key words:** methods: analytical — methods: statistical — galaxies: haloes — dark matter

## 1 INTRODUCTION

Hierarchical structure formation in a  $\Lambda$ CDM cosmology gives rise to dark matter haloes with abundant substructure in the form of self-bound clumps of matter. These subhaloes are the remnants of dark matter haloes that have been accreted by their host halo over cosmic time, and that have (thus far) survived tidal destruction. Dark matter subhaloes host satellite galaxies, boost the dark matter annihilation signal, cause tidal heating of stellar streams and disks, and are responsible for time-delays and flux-ratio anomalies in gravitational lensing. Hence, characterizing the abundance, spatial distribution and internal structure of dark matter substructure is important for a large number of astrophysical applications.

Given the highly non-linear nature of hierarchical structure formation, the substructure of dark matter haloes is best studied using high-resolution  $N$ -body simulations. Ever since the first numerical simulations reached sufficient resolution to resolve dark matter subhaloes (Tormen 1997; Ghigna et al. 1998; Tormen, Diaferio & Syer 1998; Klypin

et al. 1999; Moore et al. 1999) numerous studies have used  $N$ -body simulations of ever increasing size and/or numerical resolution to study their statistics as function of host halo mass, redshift, cosmology, and other properties of relevance, such as the formation time of the halo (e.g., Springel et al. 2001, 2008; Stoehr et al. 2002; Gao et al. 2004; De Lucia et al. 2004; Diemand, Moore & Stadel 2004; Gill et al. 2004a,b; Kravtsov et al. 2004; Reed et al. 2005; Shaw et al. 2007; Giocoli et al. 2008a, 2010; Weinberg et al. 2008; Angulo et al. 2009; Boylan-Kolchin et al. 2010; Klypin, Trujillo-Gomez & Primack 2011; Wu et al. 2013). These studies not only used different simulation codes, different cosmologies, different numerical resolutions, and different simulation volumes, but also different subhalo finders.

To date, more than a dozen different subhalo finders have been used, all based on some of the following two characteristics of a subhalo: (i) it is a self-bound, overdense region inside its host halo, and (ii) it was its own host halo before it merged into its current host (see Han et al. 2012). Most halo finders only use the instantaneous particle positions and velocities to identify subhaloes based on the first characteristic listed above. Most of these only use the velocity information to remove unbound particles from a list of candidate particles identified based on density

\* E-mail: frank.vandenbosch@yale.edu

alone. Examples of such halo finders are **SUBFIND** (Springel et al. 2001), **SKID** (Stadel 2001), Bound Density Maximum (BDM; Klypin & Holtzman 1997), Amiga Halo Finder (AHF; Knollmann & Knebe 2009), and Voronoi Bound Zones (VOBOZ; Neyrinck, Gnedin & Hamilton 2005). Others, such as 6-Dimensional Friends-of-Friends (6DFOF; Diemand Kühlen & Madau 2006), Hierarchical Structure Finder (HSF; Maciejewski et al. 2009) and **ROCKSTAR** (Behroozi et al. 2013a), identify (sub)haloes using the full six-dimensional phase-space information. Finally, there are also subhalo finders that make additional use of the second characteristic listed above by employing the time domain. Since subhaloes are remnants of dark matter host haloes, one can identify the former by tracing the member particles of the latter that remain part of a self-bound entity. Examples of these are **SURV** (Tormen et al. 1998) and the Hierarchical Bound-Tracing algorithm (**HBT**) of Han et al. (2012). Note that **ROCKSTAR** also uses some time-domain information in its (sub)halo identification, making it the only subhalo finder that uses information in seven dimensions.

In an era of precision cosmology, in which accurate, percent level characterization of the abundances of dark matter haloes and subhaloes is crucial, it is of paramount importance to compare the performance of all these different subhalo finders, and to quantify their accuracy and reliability. Unfortunately, and somewhat surprisingly, this has received relatively little attention. Muldrew, Pearce & Power (2011) compared the performances of **SUBFIND** and **AHF** in recovering mock subhaloes placed in a mock host halo. They showed that the mass of the subhalo recovered by **SUBFIND** has a strong dependence on its radial position within the host halo, and that neither subhalo finder can accurately recover the subhalo mass when it is near the center of the host halo. More quantitatively, **SUBFIND** was only able to recover 50 percent of the subhalo mass when its center is located at half the virial radius from the center of its host. At  $r < r_{\text{vir}}/10$ , neither subhalo finder could recover more than 40 percent of the actual subhalo mass. These problems arise from the subhalo being defined as a mere overdensity in configuration space. Indeed, using a similar approach based on mock haloes, Knebe et al. (2011) showed that this problem can be significantly reduced (but not eliminated) when using a subhalo finder that operates in 6D phase-space. A potential problem with these two studies, though, is that they used mock haloes. As pointed out in Knebe et al. (2011), the discrepancy between the true and recovered subhalo masses is likely to be overestimated in this idealized setup. In reality, a subhalo experiences tidal stripping and truncation when moving towards the center of its host halo, and the mass discrepancy is likely to be reduced when only considering the mass within the tidal truncation radius. Following up on the initial study by Knebe et al. (2011), Onions et al. (2012) therefore compared the performance of subhalo finders using an ultra-high resolution simulation of a single Milky-Way sized dark matter halo from the Aquarius project (Springel et al. 2008). Comparing the statistics and properties of the dark matter subhaloes identified within this single host halo with ten different subhalo finders, and using a common post-processing pipeline to uniformly analyze the particle lists provided by each finder, they find that the basic properties (mass and maximum circular velocity) of dark matter subhaloes can be reliably recovered (at an accuracy better than

20 percent) if the subhaloes contain more than 100 particles. In a follow-up study, Knebe et al. (2013) showed that discarding the results from the two subhalo finders that lack a (reliable) procedure to remove unbound particles, the scatter among the (eight remaining) subhalo finders is reduced by a factor two, to  $\sim 10\%$ . Finally, the studies of Onions et al. (2012) and Knebe et al. (2013) show that configuration finders yield less reliable masses for subhaloes close to the center of their host than phase-space finders, but that the differences are significantly smaller than suggested by the tests based on mock haloes described above.

Unfortunately, since the study by Onions et al. only used a single dark matter halo, albeit at exquisite numerical resolution, the comparison is limited to the relatively low mass end of the subhalo mass function, where the cumulative mass function  $N(> m)$ , exceeds unity. In order to study the massive end of the subhalo mass function, where  $N(> m) < 1$ , one needs to average over large numbers of host haloes. The abundances of these rare but massive subhaloes has important implications for, among others, the statistics of massive satellite galaxies (e.g., Boylan-Kolchin et al. 2010; Busha et al. 2011) and the detection rate of dark matter substructure via gravitational lensing (e.g., Vegetti et al. 2010, 2012). In this paper we use subhalo mass functions and subhalo catalogs from a variety of numerical simulations that are publicly available, and that have been obtained using different subhalo finders, to compare subhalo mass functions, focusing on the massive end. We confirm the findings by Onions et al., that the subhalo mass functions are consistent at the 20 percent level at the low-mass end. At the massive end, though, different subhalo finders yield subhalo abundances that differ by more than one order of magnitude! By comparing the simulation results with a new, semi-analytical model (Jiang & van den Bosch 2014b), we demonstrate that subhalo finders that identify subhaloes based purely on density in configuration space, such as the popular **SUBFIND** and **BDM**, dramatically underpredict the masses, but not the maximum circular velocities, of massive subhaloes. We also show that the model predictions are in excellent agreement with the simulation results when they are analyzed using more advanced subhalo finders that use phase-space and/or time domain information in the identification of subhaloes. We discuss a number of implications of our findings, in particular with regard to the power-law slope of the subhalo mass and velocity functions.

Throughout we use  $m$  and  $M$  to refer to the masses of subhaloes and host haloes, respectively, use  $\ln$  and  $\log$  to indicate the natural logarithm and 10-based logarithm, respectively, and express units that depend on the Hubble constant in terms of  $h = H_0/(100 \text{ km s}^{-1} \text{ Mpc}^{-1})$ .

## 2 DESCRIPTION OF DATA AND MODEL

The main goal of this paper is two-fold. First, we wish to compare mass and velocity functions of dark matter subhaloes obtained from numerical simulations using different subhalo finders among each other, in order to gauge their robustness. Second, we want to compare these simulation results to predictions from the new, semi-analytical model of Jiang & van den Bosch (2014b) in order to assess its reliability. This section describes the various numerical simula-

tions and subhalo finders used in our comparison, followed by a brief description of our semi-analytical model.

## 2.1 Numerical Simulations

Table 1 lists the various simulations used in this paper. More details regarding each of these simulations can be found in the references listed in the final column. In the case of the Bolshoi and MultiDark simulations we use publicly available halo catalogs to construct our own subhalo mass and velocity functions. In the case of the other simulations, we use published results, mainly in the form of fitting functions. As is evident from Table 1, all these simulations adopt flat  $\Lambda$ CDM cosmologies, but with slightly different values for the cosmological parameters. However, as we will show below, these mild differences in cosmology have a negligible impact on the subhalo mass functions, and one can therefore compare results from these simulations without having to make any corrections for differences in cosmology.

## 2.2 Subhalo Finders

The subhalo mass functions presented below have been obtained using four different subhalo finders: **SUBFIND**, **BDM**, **ROCKSTAR** and **SURV**. We briefly describe each of these subhalo finders in turn, but refer the reader to the original papers, referenced below, for more details.

### 2.2.1 Bound-Density-Maximum

The Bound-Density-Maximum (**BDM**) algorithm, developed by Klypin & Holtzman (1997), identifies both host haloes (also called ‘distinct’ haloes) and subhaloes (see also Riebe et al. 2013). It locates density maxima in the particle distribution and uses an iterative scheme to remove unbound particles. As described in Appendix A of Klypin et al. (2011), if two haloes are (i) separated by less than one virial radius, (ii) have masses that differ by less than a factor of 1.5, and (iii) have a relative velocity less than 0.15 of the rms velocity of dark matter particles inside the haloes, **BDM** removes the smaller halo and keeps only the larger one. As we show below, and as anticipated in Klypin et al. (2011), this ‘correction’, which was introduced “to remove a defect of halo-finding where the same halo is identified more than once” results in systematic errors in the subhalo mass function at the massive end, especially in more massive host haloes (which assembled more recently). In this paper we use **BDM** catalogs obtained from both the Bolshoi and MultiDark simulations.

### 2.2.2 SUBFIND

The **SUBFIND** algorithm, developed by Springel et al. (2001), is similar to **BDM** in that it identifies substructures within a host halo by searching for overdense regions using a local density estimate, obtained by kernel interpolation over the nearest neighbors. It identifies substructure candidates as regions bounded by an isodensity surface that traverses a saddle point of the density field and uses an iterative unbinding procedure to ensure that these potential substructures are physically bound. **SUBFIND** has been used extensively in

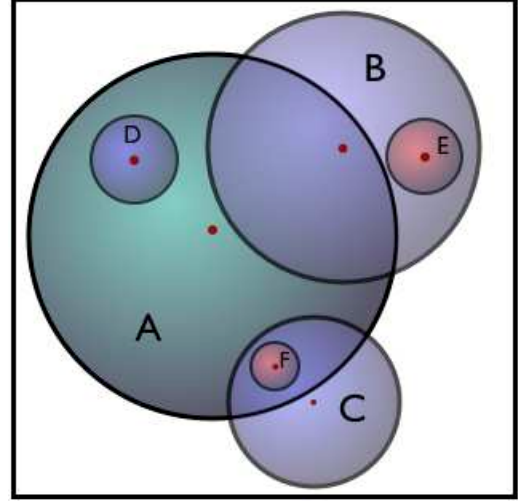


**Figure 1.** Illustration of overlapping (spherical) haloes. The small red dots indicate the halo centers. Since the centers of B, D and F are all located within the extent of A, most subhalo finders will consider them subhaloes of A. Note, though, that B lies partially outside of A, so that not all of B’s mass is considered part of A, at least not in **ROCKSTAR** and **BDM**. Halo E is a subhalo of B, which makes it a second-order subhalo of A. However, since its center falls outside of A, **ROCKSTAR** and **BDM** do not count it as such. Finally, F is a first-order subhalo of C, and will be counted as such in the semi-analytical model. However, since its center falls inside of A, while that of C doesn’t, both **ROCKSTAR** and **BDM** will consider F a first-order subhalo of both A and C. See §2.4 for a detailed discussion.

analyzing the Millennium simulations (Boylan-Kolchin et al. 2009, 2010; Gao et al. 2011), the Aquarius simulations (Springel et al. 2008), and the Phoenix simulations (Gao et al. 2012). In what follows we use some of these results (mainly in the form of published fitting functions) for comparison.

### 2.2.3 ROCKSTAR

**ROCKSTAR** (Robust Overdensity Calculation using K-Space Topologically Adaptive Refinement) is a phase-space halo finder designed to maximize halo consistency across time-steps (Behroozi et al. 2013a,b). It uses adaptive hierarchical refinement of friends-of-friends groups in six phase-space dimensions and one time dimension, resulting in a very robust tracking of substructure (see Knebe et al. 2011, 2013). **ROCKSTAR** has been used to analyze, among others, the Bolshoi, MultiDark and Rhapsody simulations.

### 2.2.4 SURV

The subhalo finder **SURV** was developed by Tormen et al. (1998), and improved upon by Tormen, Moscardini & Yoshida (2004) and Giocoli et al. (2008a). It identifies subhaloes within the virial radius of a final host halo by following their progenitors from the time they were first accreted by the host’s main progenitor. Hence, **SURV** differs from the methods discussed above, in that it uses prior information based on the host halo’s merger history to identify its subhaloes. In particular, subhaloes are identified as those sub-

**Table 1.** Numerical Simulations used in this Paper

Simulation (1)	$\Omega_{m,0}$ (2)	$\Omega_{\Lambda,0}$ (3)	$\Omega_{b,0}$ (4)	$\sigma_8$ (5)	$n_s$ (6)	$h$ (7)	$L_{\text{box}}$ (8)	$N_p$ (9)	$m_p$ (10)	Reference (11)
Bolshoi	0.27	0.73	0.047	0.82	0.95	0.70	250	2048 <sup>3</sup>	$1.4 \times 10^8$	Klypin et al. (2011)
MultiDark	0.27	0.73	0.047	0.82	0.95	0.70	1000	2048 <sup>3</sup>	$8.6 \times 10^9$	Prada et al. (2012)
Millennium I	0.25	0.75	0.045	0.90	1.0	0.73	500	2160 <sup>3</sup>	$8.6 \times 10^8$	Springel et al. (2005)
Millennium II	0.25	0.75	0.045	0.90	1.0	0.73	100	2160 <sup>3</sup>	$6.9 \times 10^6$	Boylan-Kolchin et al. (2010)
Millennium HS	0.25	0.75	0.045	0.90	1.0	0.73	100	900 <sup>3</sup>	$9.5 \times 10^7$	Angulo et al. (2009)
Aquarius	0.25	0.75	0.045	0.90	1.0	0.73	zoom-in	zoom-in	$> 1.7 \times 10^3$	Springel et al. (2008)
Phoenix	0.25	0.75	0.045	0.90	1.0	0.73	zoom-in	zoom-in	$> 6.4 \times 10^5$	Gao et al. (2012)
Rhapsody	0.25	0.75	0.040	0.80	1.0	0.73	zoom-in	zoom-in	$1.3 \times 10^8$	Wu et al. (2013)
GIF2	0.30	0.70	0.040	0.90	1.0	0.70	110	400 <sup>3</sup>	$1.7 \times 10^9$	Gao et al. (2004)

Parameters of the various numerical simulations discussed in this paper. Columns (2) - (7) list the present-day cosmological density parameters for the matter,  $\Omega_{m,0}$ , the cosmological constant,  $\Omega_{\Lambda,0}$ , and the baryonic matter,  $\Omega_{b,0}$ , the normalization,  $\sigma_8$ , and spectral index,  $n_s$ , of the matter power spectrum, and the Hubble parameter,  $h = H_0/(100 \text{ km s}^{-1} \text{ Mpc}^{-1})$ . Columns (8) - (10) list the box size of the simulation,  $L_{\text{box}}$ , (in  $h^{-1} \text{ Mpc}$ ), the number of particles used,  $N_p$ , and the particle mass,  $m_p$  (in  $h^{-1} \text{ M}_\odot$ ), respectively. Note that Aquarius, Phoenix and Rhapsody are ensembles of high-resolution zoom-in simulations of MW-sized (Aquarius) and cluster-sized (Phoenix & Rhapsody) haloes. More details regarding each simulation can be found in the references listed in Column (11).

sets of particles that belonged to one and the same progenitor halo at its moment of accretion (i.e., when it first became a subhalo) that are still part of a self-bound entity within the corresponding tidal radius (see §2.4 below). **SURV** is very similar to the Hierarchical Bound Tracing (**HBT**) method recently developed by Han et al. (2012). In this paper we use the subhalo mass functions obtained by Giocoli et al. (2008a) using a **SURV** analysis of the GIF2 simulation.

### 2.3 Analytical Model

In addition to the simulation results mentioned above, we also include in our comparison results from the semi-analytical model developed by the authors, and described in detail in our companion paper (Jiang & van den Bosch 2014b; hereafter Paper I). Starting from halo merger trees, this model uses a simple semi-analytical description for the *average* subhalo mass loss rate (where the average is taken over all orbital energies, orbital angular momenta and orbital phases) to evolve the masses of dark matter subhaloes from the moment of accretion to  $z = 0$ . It is a modified and improved version of the model developed by van den Bosch, Tormen & Giocoli (2005). The main improvement is that the merger trees are constructed using the algorithm developed by Parkinson, Cole & Helly (2008), which, as discussed in Jiang & van den Bosch (2014a), is far more reliable than the Somerville & Kolatt (1999) method used in van den Bosch et al. (2005). In addition, it uses an improved model for the subhalo mass loss rate that is calibrated against numerical simulations, includes scatter in the mass loss rates that arises from the variance in orbital energies and angular momenta, and treats the entire hierarchy of substructure, including sub-subhaloes, sub-sub-subhaloes, etc. As shown in Paper I, this model can accurately reproduce the subhalo mass functions obtained by Giocoli et al. (2008a) and Wu et al. (2013) using the GIF2 and Rhapsody simulations, respectively. One of the main goals of this paper is to compare this simple and fast semi-analytical model to other simulation results.

In addition to subhalo masses, the semi-analytical

model of Jiang & van den Bosch (2014b) also yields the maximum circular velocities,  $V_{\text{max}}$ , for both host haloes and subhaloes. For host haloes,  $V_{\text{max}}$  is computed assuming that the density distribution of dark matter haloes follow a NFW profile (Navarro, Frenk & White 1997), so that

$$V_{\text{max}} = 0.465 V_{\text{vir}} \sqrt{\frac{c}{\ln(1+c) - c/(1+c)}}, \quad (1)$$

where  $c$  is the halo's concentration parameter, and

$$V_{\text{vir}} = 159.43 \text{ km s}^{-1} \left( \frac{M}{10^{12} h^{-1} \text{ M}_\odot} \right)^{1/3} \left[ \frac{H(z)}{H_0} \right]^{1/3} \left[ \frac{\Delta_{\text{vir}}(z)}{178} \right]^{1/6}, \quad (2)$$

is the virial velocity of a dark matter halo of virial mass  $M$  at redshift  $z$ . Here  $H(z)$  is the Hubble parameters, and  $\Delta_{\text{vir}}(z)$  specifies the average density of a collapsed dark matter halo in units of the critical density,  $\rho_{\text{crit}}$ , and is well represented by the fitting function of Bryan & Norman (1998):

$$\Delta_{\text{vir}}(z) = 18\pi^2 + 82x - 39x^2, \quad (3)$$

where  $x = \Omega_m(z) - 1$ . For the cosmologies used in this paper  $\Delta_{\text{vir}} \sim 100$ . It is well known that the halo concentration is strongly correlated with the halo's assembly history, to the extent that more concentrated haloes assemble earlier (e.g., Navarro et al. 1997; Wechsler et al. 2002; Giocoli, Tormen & Sheth 2012; Ludlow et al. 2013). We use the model of Zhao et al. (2009), according to which

$$c(M, t) = 4.0 \left[ 1 + \left( \frac{t}{3.75 t_{0.04}} \right)^{8.4} \right]^{1/8}. \quad (4)$$

Here  $t_{0.04}$  is the proper time at which the host halo's main progenitor gained 4% of its mass at proper time  $t$ , which we extract from the halo's merger tree (see Paper I for details). For subhaloes, we compute  $V_{\text{max}}$  using

$$V_{\text{max}} = 2^\mu V_{\text{acc}} \frac{(m/m_{\text{acc}})^\eta}{(1 + m/m_{\text{acc}})^\mu}, \quad (5)$$

where  $m_{\text{acc}}$  and  $V_{\text{acc}}$  are the subhalo mass and maximum

circular velocity at the time of accretion, and  $(\eta, \mu) = (0.44, 0.60)$ . As described in detail in Paper I, this relation between  $V_{\max}/V_{\text{acc}}$  and  $m/m_{\text{acc}}$  is obtained by fitting data from the Rhapsody simulations (Wu et al. 2013), and, as we demonstrate below, also adequately describes the data from the Bolshoi and MultiDark simulations. As shown in Paper I, implementing this ‘recipe’ for  $V_{\max}$  yields subhalo velocity functions,  $dN/d\log(V_{\max}/V_{\text{vir}})$ , where  $V_{\text{vir}}$  is the virial velocity of the host halo, in excellent agreement with the simulation results of Wu et al. (2013).

## 2.4 Definition of (Sub)Halo Mass

A recurring source of contention in this paper is the exact definition of (sub)halo mass. Therefore, as a preamble, we now discuss (some of) the various definitions that are used here and in the literature.

Throughout this study we focus on results at  $z = 0$ , and we define all *host* haloes of mass  $M$  as spheres with an average density  $\rho_h \equiv 3M/4\pi r_{\text{vir}}^3 = \Delta_{\text{vir}}\rho_{\text{crit}}$ , where  $r_{\text{vir}}$  is the virial radius. We follow the nomenclature of Paper I and refer to subhaloes that were accreted directly onto the main progenitor of the host halo as first-order subhaloes. Similarly, haloes that accrete directly onto the progenitors of first-order subhaloes give rise to second-order subhaloes (or sub-subhaloes), and the same logic is used to define progenitors and subhaloes of third order and higher.

In the case of our semi-analytical model, we define subhalo masses as the fraction of the virial mass the progenitor had at accretion that has not been stripped off (as described by our mass-loss model). Hence, in our model subhalo mass always decreases with time, and we ignore the possibility that two subhaloes may merge. Also, the model treats all masses as ‘inclusive’, including in each (sub)halo mass the mass of all its substructure. This implies that a single dark matter particle can be part of multiple sub-structures (of different order). Note that, in this case, the fraction of host halo mass that is locked up in substructure is obtained by integrating the SHMF of first-order subhaloes only.

The subhalo finders **ROCKSTAR** and **BDM** use the same definitions of subhalo mass. After the finder has identified the set,  $\mathcal{S}$ , of particles that belong to a self-bound substructure, the center of the subhalo is identified as the location of its most bound particle (here the potential is computed using solely the particles in  $\mathcal{S}$ ). The mass of the subhalo is defined as the sum over all particles in  $\mathcal{S}$  that fall within a radius  $r_{\text{vir}}$  of this center, where  $r_{\text{vir}}$  is defined above. Hence, the subhalo mass can be less than the mass of all particles in  $\mathcal{S}$ . Both **ROCKSTAR** and **BDM** are similar to our semi-analytical model in that their (sub)halo masses are always ‘inclusive’. However, some non-trivial issues can arise when (sub)haloes overlap. As an example, consider the situation illustrated in Fig. 1. Here B is a subhalo of A, since its center is located within the virial radius of A. However, only the mass of B that is located within that same radius is counted towards the mass of A. Hence, in this case, where A and B have comparable mass, the mass ratio,  $m/M$ , of subhalo mass to host halo mass can exceed 0.5. Note that this is not possible in the case of our semi-analytical model. As we will see, this results in subtle differences at the massive end of the subhalo mass functions. Note also that although halo E in Fig. 1 is a subhalo of B, it is not counted as a sub-subhalo of A in

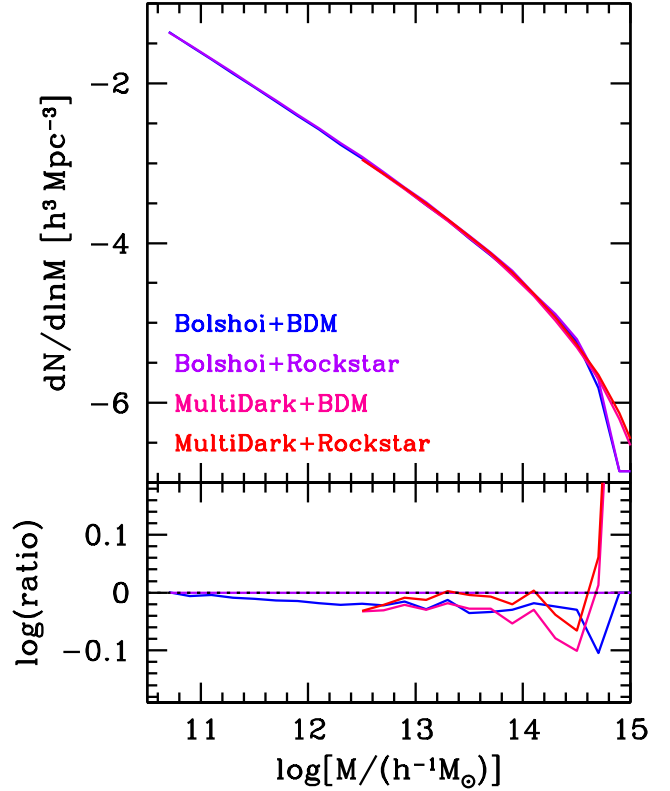


**Figure 2.** Mass functions of dark matter host haloes. Results are shown for both the Bolshoi and MultiDark simulations analyzed using both **BDM** and **ROCKSTAR** (as indicated). The lower panel plots the logarithm of the ratio of these mass functions with respect to that of Bolshoi+**ROCKSTAR**, and shows that the various mass functions are in excellent agreement. There are some differences between MultiDark and Bolshoi at the massive end due to sample variance, but overall the **ROCKSTAR** and **BDM** results agree at the 10 to 20 percent level.

the **ROCKSTAR** and **BDM** halo catalogs because its center does not fall within the virial radius of A. This is despite the fact that B is considered a subhalo of A. Even more tricky is the issue of halo F. Before C started to overlap with A, F was an unambiguous subhalo of C. Since the center of C hasn’t yet entered the virial radius of A, our semi-analytical model still considers F to be a first-order subhalo of C, unassociated with A. However, since F falls inside of A, most subhalo finders will count F as a first-order subhalo of *both* C and A. These non-trivial differences in assigning masses and orders to subhaloes can be responsible for subtle differences in the mass functions of (higher-order) subhaloes.

In the case of **SURV**, we follow the definition of Giocoli et al. (2008a) in which the mass of a subhalo is simply defined as the mass of the subset of particles that belonged to the virial mass of a progenitor halo at its moment of accretion (i.e., when it first became a subhalo) that are still part of a self-bound entity within the corresponding tidal radius. As for **ROCKSTAR** and **BDM**, these (sub)halo masses are ‘inclusive’.

Finally, in the case of **SUBFIND**, the mass of a subhalo is defined as the mass of all self-bound particles located within the isodensity surface that bounds the object. **SUBFIND** masses differ from all other masses discussed above in that they are ‘exclusive’: the mass of a sub-subhalo is not

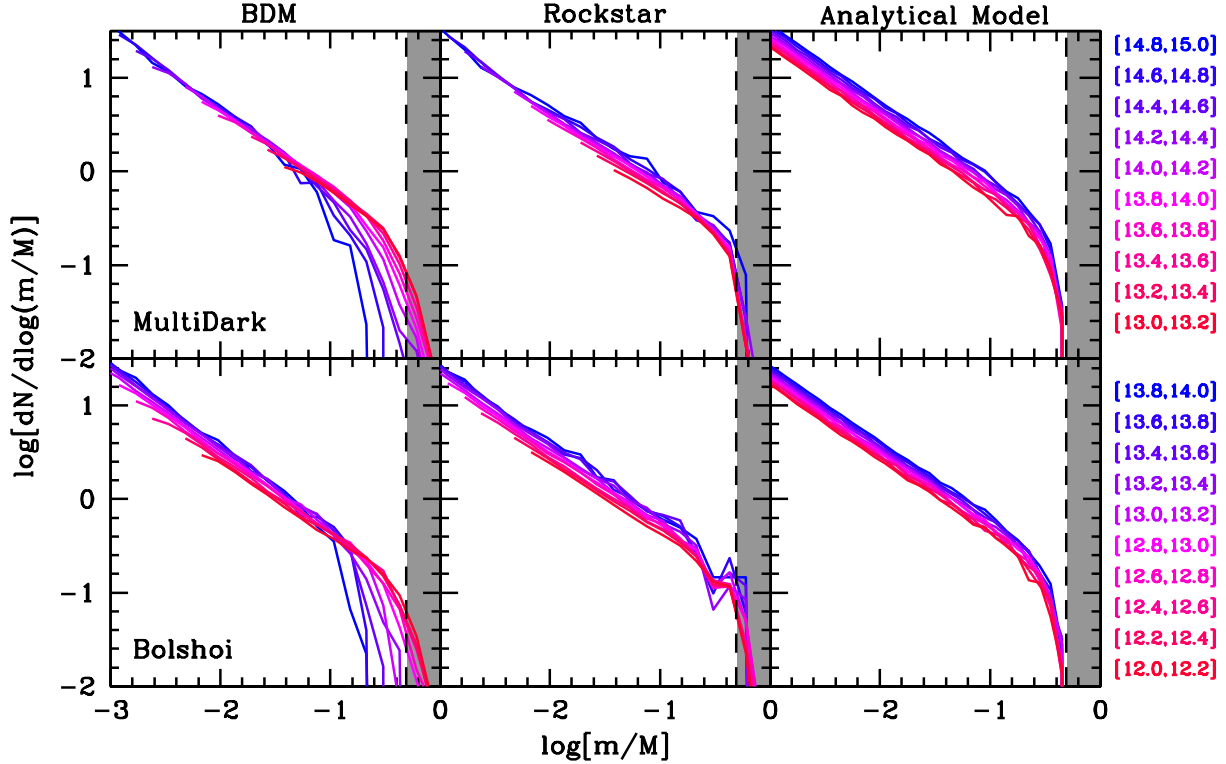


**Figure 3.** Subhalo mass functions,  $dN/d\log(m/M)$ , for dark matter host haloes in different mass bins (different colors), as function of the subhalo mass,  $m$ , normalized to the host halo mass,  $M$ . The values in square brackets at the right side indicate the range in host halo mass  $\log[M/(h^{-1} M_{\odot})]$ . Panels in left and middle columns show SHMFs obtained using the subhalo finders BDM and SUBFIND applied to the MultiDark (upper panels) and Bolshoi (lower panels) simulations. Results are only shown for subhaloes that contain at least 50 particles, which explains why less massive host haloes have their SHMF restricted to a more limited dynamic range in  $m/M$ . For comparison, the SHMFs shown in the right-hand panel have been obtained using our semi-analytical model, averaging over 10,000 host haloes as described in the text. The gray regions at the right side of each panel indicate where  $m/M > 0.5$ , which is a forbidden region for our semi-analytical model, but not for the simulations (see discussion in §2.4).

included in the mass of its ‘hosting’ subhalo. Consequently, integrating  $dN/d(m/M)$  for first-order subhaloes does *not* yield the mass fraction in substructure, which instead requires integrating the SHMF of *all* orders of subhaloes. We emphasize, though, that the difference between ‘inclusive’ and ‘exclusive’ masses is small, and does not have a significant impact on the SHMFs. This is easy to understand; subhaloes typically account for only about  $\sim 10$  percent of the mass of a host halo. Similarly, sub-subhaloes only account for  $\lesssim 10$  percent of the mass of a subhalo, etc. Hence, the difference between inclusive and exclusive can cause differences of up to  $\sim 10$  percent in the masses of individual subhaloes, which does not have a significant impact on  $dN/d\log(m/M)$ , at least not compared to the differences we are concerned with in this paper (see also Onions et al. 2012).

### 3 RESULTS

We start our investigation by comparing the  $z = 0$  subhalo mass functions obtained from our semi-analytical model with those obtained from the Bolshoi and MultiDark simulations using both BDM and ROCKSTAR. The Bolshoi halo cat-

alogs are publicly available at the Bolshoi website<sup>†</sup>, which also lists the ROCKSTAR catalogs for the MultiDark simulation. The BDM catalog for the MultiDark simulation is downloaded from the MultiDark website<sup>‡</sup>. For each host halo, the catalogs contain the present-day virial mass,  $M$ , and maximum circular velocity,  $V_{\max}$ . In the case of subhaloes, the output contains the present-day mass of the subhalo,  $m$ , its maximum circular velocity,  $V_{\max}$ , as well as the virial mass,  $m_{\text{acc}}$ , and maximum circular velocity,  $V_{\text{acc}}$ , of the subhalo at the time of accretion.

Before comparing subhalo statistics, it is useful to check that the different simulations and halo finders yield consistent abundances of *host* haloes. Fig. 2 compares the halo mass functions of host haloes in MultiDark and Bolshoi, as obtained with both ROCKSTAR and BDM. As is evident, the agreement is excellent. The Bolshoi results deviate from the MultiDark results at the massive end, but this is a manifestation of sample variance arising from the limited box sizes. Overall, the abundances obtained using ROCKSTAR and BDM agree with each other at the 10 to 20 percent level, in good agreement with the results of Knebe et al. (2011).

<sup>†</sup> <http://hipacc.ucsc.edu/Bolshoi/MergerTrees.html>

<sup>‡</sup> <http://www.multidark.org/MultiDark/>



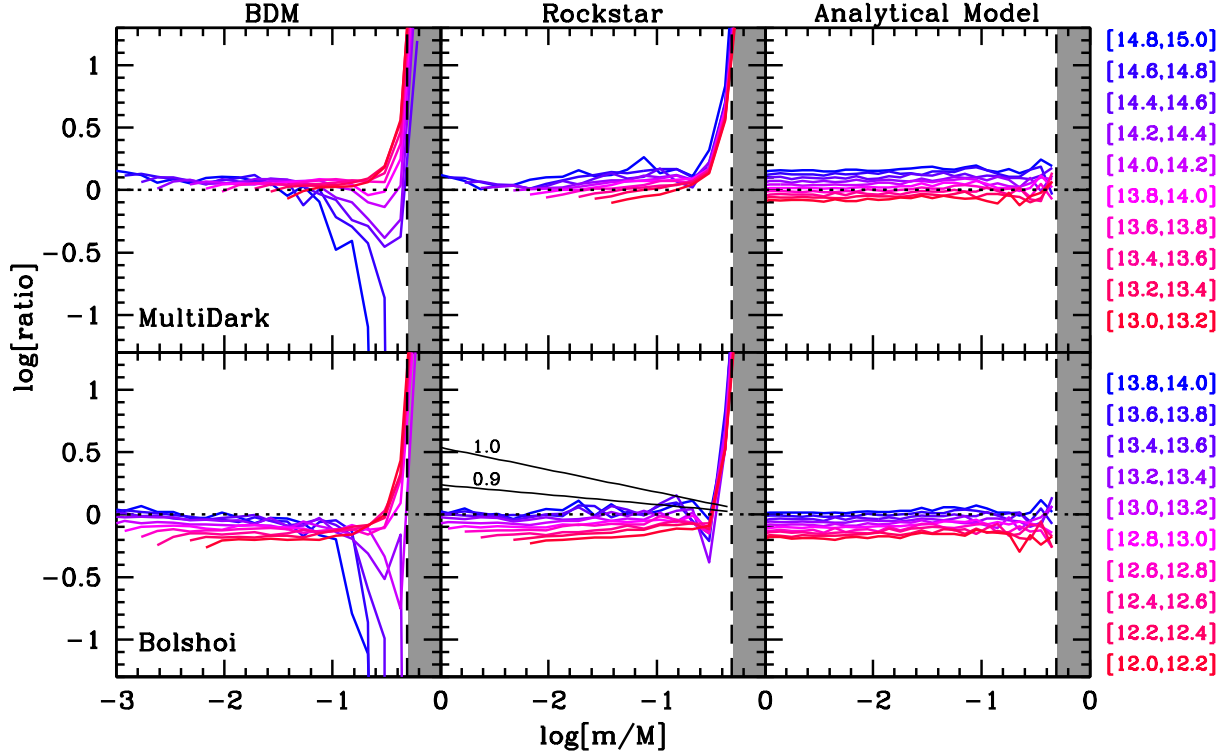


**Figure 4.** Same as Fig. 3, except that here we show the logarithm of the ratio between the SHMF,  $dN/d\log(m/M)$ , and the fiducial SHMF given by Eq. (6) with slope  $\alpha = 0.82$  and normalization  $A_M = 0.09$ . Note the good agreement for  $\log[m/M] \lesssim -1$ , and the large differences at the massive end. The black, solid lines in the lower, middle panel indicate the residuals that would arise if the SHMF has the form of Eq. (6), but with  $\alpha = 0.9$  and  $1.0$ , as labeled. This shows that the power-law slopes of the SHMFs are clearly less steep than  $0.9$ , contrary to numerous claims in the literature (see text for a detailed discussion).

### 3.1 Subhalo Mass Functions: Bolshoi & MultiDark

We now turn our attention to subhaloes. Using all haloes and subhaloes with at least 50 dark matter particles, we compute the SHMFs,  $dN/d\log(m/M)$ , for 10 different bins in host halo mass, each with a bin width of 0.2 dex. In the case of MultiDark we use logarithmic mass bins  $\log[M/(h^{-1} M_\odot)] \in [13 + 0.2(n-1), 13 + 0.2n]$  with  $n = (1, 2, \dots, 10)$ , while for the smaller but higher-resolution Bolshoi simulation, we adopt  $[12 + 0.2(n-1), 12 + 0.2n]$ . When counting subhaloes, we include subhaloes of all orders (i.e., subhaloes, sub-subhaloes, etc.). The resulting SHMFs are shown in Fig. 3: upper and lower panels correspond to MultiDark and Bolshoi, respectively, while panels in the left and middle columns show the results obtained using the BDM and ROCKSTAR catalogs, respectively. Different colors correspond to different bins in host halo mass, as indicated. For comparison, the right-hand panels show the SHMFs obtained using our semi-analytical model averaged over 10,000 host haloes with masses  $\log[M/(h^{-1} M_\odot)] = 13.1 + 0.2n$  (MultiDark) and  $12.1 + 0.2n$  (Bolshoi). Here we have adopted the same cosmology as for the simulations (see Table 1), and again the SHMFs include subhaloes of all orders. The gray area at the right side of each panel marks the region where  $m/M > 0.5$ ; no subhalo in our semi-analytical model can have a mass this large. However, as is evident, some of the ROCKSTAR and BDM SHMFs do extent into this regime. As discussed in §2.4,

this as a consequence of their treatment of sub-haloes that are not entirely located within their host halo.

In order to facilitate a more detailed comparison, Fig. 4 shows the ratios of all these SHMFs with respect to a fiducial SHMF given by

$$\frac{dN}{d\log(m/M)} = A_M \left(\frac{m}{M}\right)^{-\alpha} \exp[-50(m/M)^4]. \quad (6)$$

with slope  $\alpha = 0.82$  and normalization  $A_M = 0.09$ . As shown in Paper I, this functional form accurately fits the SHMFs predicted by our semi-analytical model, while the normalization parameter  $A_M$  is a function of halo mass, redshift and cosmology. This is also evident from the right-hand panels of Figs. 3 and 4, which show that the functional form of the model SHMF is invariant, but that more massive haloes have more substructure (i.e., a larger normalization  $A_M$ ). This arises because (i) the *unevolved* subhalo mass function (i.e., the mass function of the subhaloes at accretion) is independent of host halo mass, and (ii) more massive haloes assemble later. Consequently, their subhaloes have, on average, been exposed to mass stripping for a shorter period of time (see also van den Bosch et al. 2005 and Paper I).

Overall, the simulation results are in good agreement with each other and with the model predictions. This is especially true at the low mass end ( $m \lesssim 0.1M$ ) where the agreement is at the level of  $\sim 20$  percent ( $\Delta \log[dN/d\log(m/M)] \lesssim 0.1\text{dex}$ ), confirming the earlier findings of Onions et al. (2012). Particularly reassuring is the fact that the simulation results reveal the same host

**Table 2.** Number of host haloes

Simulation	Algorithm	[12, 12.5]	[13, 13.5]	[14, 14.5]
Bolshoi	ROCKSTAR	37,498	4,281	283
Bolshoi	BDM	35,889	4,046	273
MultiDark	ROCKSTAR	–	267,745	17,699
MultiDark	BDM	–	256,399	16,342
MSII	SUBFIND	2,039	–	–
GIF2	SURV	3,349	461	35

Number of host haloes used for the SHMFs shown in Fig. 5. Columns (1) and (2) indicate the simulation and subhalo finder, while columns (3) - (5) list the number of host haloes in the mass bin indicated at the top, where the values in square brackets mark the range in  $\log[M/(h^{-1} \text{ M}_\odot)]$ .

halo mass dependence as predicted by our model (see also Gao et al. 2004 and Shaw et al. 2006). Note, though, that for some unknown reason, the SHMFs obtained from the MultiDark+BDM analysis do not reveal any significant dependence on host halo mass at the low mass end.

Another important result is that all SHMFs agree, to good accuracy, on the slope at the low-mass end,  $\alpha$ , which is equal to 0.82 in the case of our semi-analytical model (see Eq. [6] and Paper I). This value for  $\alpha$  falls roughly midway of the values reported by studies based on numerical simulations, which span the entire range from 0.7 to 1.1 (Moore et al. 1999; Ghigna et al. 1999; Helmi et al. 2002; De Lucia et al. 2004; Gao et al. 2004; Shaw et al. 2006; Diemand, Kuhlen & Madau 2007; Angulo et al. 2009; Giocoli et al. 2010). There are a number of reasons for this large spread in measured slopes. Foremost, earlier studies lacked sufficient numerical resolution and/or statistics, and where only able to fit the slope of the SHMF over a limited range in mass. In addition, many of these studies fitted the SHMF with a single power-law, without an exponential tail, which tends to bias the slope high. And finally, some of the discrepancy arises from the use of different subhalo finders. In particular, in a recent study of Milky Way sized haloes extracted from the Millennium II (Boylan-Kolchin et al. 2009) and Aquarius (Springel et al. 2008) simulations, Boylan-Kolchin et al. (2010) used SUBFIND to infer a slope  $\alpha = 0.94$ . Gao et al. (2012), using SUBFIND to analyze nine high-resolution simulations of cluster-sized haloes that are part of the ‘Phoenix Project’, inferred an even steeper slope of  $\alpha = 0.98$ , very close to the critical value of unity for which each logarithmic mass bin contributes equally to the total mass in substructure. Such a steep slope is not only inconsistent with our model predictions, but also with the BDM and ROCKSTAR results shown, all of which suggest that  $0.78 \lesssim \alpha \lesssim 0.84$ . To emphasize this level of inconsistency, the thin, solid lines in the middle, lower panel of Fig. 4 correspond to Eq. (6) but with  $\alpha = 0.9$  and 1.0, as indicated. We believe that this discrepancy is due to issues with SUBFIND, which, as we demonstrate below, yields SHMFs that strongly deviate from most other subhalo finders, especially at the massive end.

Although Figs. 3 and 4 indicate a good level of agreement among simulations and model for subhaloes with  $m/M \lesssim 0.1$ , the situation is less cheerful at the massive end, not probed by the comparison study of Onions et

al. (2012). Whereas ROCKSTAR yields SHMFs that show very little dependence on host halo mass at the exponential tail of  $dN/d \log(m/M)$ , in excellent agreement with the predictions of our semi-analytical model, the BDM results are very different. In particular, BDM yields SHMFs for which the abundance of massive subhaloes declines strongly with increasing host halo mass. In host haloes with  $M \gtrsim 3 \times 10^{14} h^{-1} \text{ M}_\odot$ , the BDM and ROCKSTAR abundances of subhaloes with  $m \gtrsim 0.3M$  differ by more than a factor three! We believe that this is an artifact of the ‘correction’ introduced in BDM to prevent the same halo from being identified more than once (see §2.2.1), and we conclude that SHMFs obtained with BDM cannot be trusted for  $m \gtrsim 0.1 M$ .

### 3.2 Subhalo Mass Functions: Subfind & Surv

Fig. 5 presents another comparison of SHMFs. Results are shown for three different mass bins:  $\log[M/(h^{-1} \text{ M}_\odot)] \in [12.0, 12.5]$  (left-hand panels),  $[13.0, 13.5]$  (middle panels) and  $[14.0, 14.5]$  (right-hand panels). The blue/purple colored lines are for the Bolshoi and MultiDark simulations analyzed with BDM and ROCKSTAR, as indicated. These SHMFs have been obtained using the same halo catalogs and methodology as in Fig. 3. The red curves are the SHMFs obtained by Giocoli et al. (2008a) using the subhalo finder SURV applied to the GIF2 simulations. The brown-red curve labeled ‘MSII+Subfind’ is the (fit to the) SHMF obtained by Boylan-Kolchin et al. (2010) using a SUBFIND analysis of the Millennium Simulation II (MSII). Since this analysis only focused on Milky-Way sized dark matter haloes, no SHMFs are available for the  $[13.0, 13.5]$  and  $[14.0, 14.5]$  mass bins. The orange lines are the SHMFs obtained by Angulo et al. (2009) using a SUBFIND analysis of both the Millennium I and Millennium HS (HS) simulations. Note that Angulo et al. (2009) define host haloes as spheres with a radius of  $r_{200c}$ , inside of which the mean density is 200 times the critical density. Hence, we need to convert their SHMFs taking account of two effects; first of all, we need to convert their host halo masses to our definition of virial mass,  $M$ , which we do assuming that dark matter haloes follow an NFW density distribution (Navarro, Frenk & White 1997) with a concentration-mass relation given by Macciò, Dutton & van den Bosch (2008). Secondly, since the volume enclosed by  $r_{200c}$  is much smaller than that enclosed by  $r_{\text{vir}}$ , we need to correct the subhalo abundances as well. We do so by simply multiplying the abundances of Angulo et al. by a factor  $(r_{\text{vir}}/r_{200c})^3$ . Although this make the oversimplified assumption that subhaloes are homogeneously distributed within their host halo, the resulting SHMF for the host mass bin  $\log[M/(h^{-1} \text{ M}_\odot)] \in [12.0, 12.5]$  is in excellent agreement with that of Boylan-Kolchin et al. (2010), which is also based on a SUBFIND analysis of the Millennium simulations<sup>§</sup>. Furthermore, the resulting SHMFs are in good agreement with the other SHMFs at the low mass end, indicating that this correction factor is appropriate. Finally, the three green lines

<sup>§</sup> If, instead, we assume that subhaloes follow the dark matter distribution, the correction factor is  $M/M_{200c}$ , which results in a  $dN/d \log(m/M)$  that is  $\sim 0.3\text{dex}$  lower than all other SHMFs shown at the low mass end.



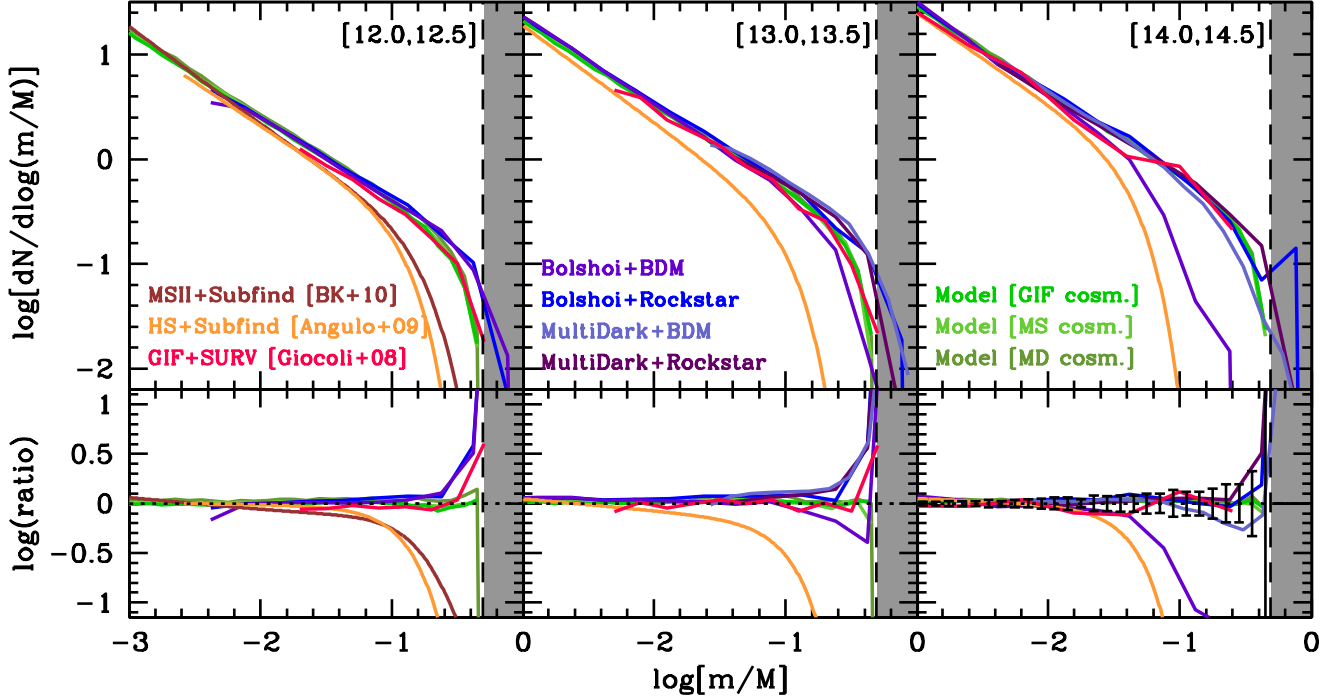


**Figure 5.** *Upper panels:* Subhalo mass functions,  $dN/d\log(m/M)$ , as function of the subhalo mass,  $m$ , normalized to the host halo mass,  $M$ . Results are shown for three bins in host halo mass,  $\log[M/(h^{-1} M_{\odot})]$ , as indicated by the values in square brackets in the upper-right corner of each column. Different curves correspond to different model predictions (green-colored curves) or simulation results (curves of other colors), as indicated. See text for a detailed discussion. *Lower panels:* Same as upper panels, except that here we show the logarithm of the ratio between the SHMF,  $dN/d\log(m/M)$ , and the fiducial SHMF given by Eq. (6) with  $A_M = 0.060$  (left panel) 0.076 (middle panel), and 0.102 (right panel).

are the semi-analytical model predictions for the cosmologies used for the GIF simulations, the Millennium simulations, and the Bolshoi/MultiDark simulations. As shown in Table 1, these cosmologies differ slightly; however, as is evident from a comparison of the three different green curves, which lie virtually on top of each other, this cosmology dependence has a completely negligible impact on the SHMFs.

The semi-analytical model predictions are obtained averaging the SHMFs of 25,000 host haloes with masses  $M = 10^{12.25} h^{-1} M_{\odot}$  (left-hand panels),  $10^{13.25} h^{-1} M_{\odot}$  (middle panels), and  $10^{14.25} h^{-1} M_{\odot}$  (right-hand panels). The numbers of host haloes used in each of the other SHMFs are listed in Table 2, except for those of Angulo et al. (2009), for which this information is not available. They range from a meager 35, in the case of the SURV SHMF for the [14.0, 14.5] mass bin to a staggering  $\sim 250,000$  for the MultiDark [13.0, 13.5] mass bin. In order to gauge how small number statistics impacts these SHMFs, we use our semi-analytical model to compute the average SHMFs of 280 host haloes, representative of the number of host haloes in the Bolshoi simulation in the [14.0, 14.5] mass bin, using 50 realizations (i.e., using 50 samples of 280 host haloes). The variance among those 50 average SHMFs is indicated by the errorbars in the lower-right panel.

Upon inspection of Fig. 5 it is clear that all SHMFs agree at the low mass end ( $m \lesssim M/100$ ) to an accuracy of  $\sim 20$  percent. This once more confirms the findings of Onions et al. (2012), who compared many more subhalo finders using a high-resolution simulation of a single host halo from the Aquarius project. However, Fig. 5 also shows

that the SUBFIND SHMFs have a steeper slope at the low mass end than all other SHMFs (this is particularly apparent for the [13.0, 13.5] mass bin), and that the agreement at the massive end of the SHMF is much weaker, especially for  $m/M \gtrsim 0.1$ . In particular;

- The ROCKSTAR SHMFs typically predict the largest abundances of massive subhaloes, even larger than those predicted by our semi-analytical model by about a factor of three for  $m/M = 0.4$ . As discussed above, the fact that the ROCKSTAR SHMFs venture into the regime with  $m/M > 0.5$  indicates that this discrepancy with respect to the semi-analytical model can largely be explained as a consequence of how sub-haloes are treated that are not entirely located within their host halo (see §2.4).
- The BDM SHMFs are generally in good agreement with those obtained with ROCKSTAR. An exception is the Bolshoi + BDM SHMF for host haloes in the [14.0, 14.5] mass bin, which dramatically underpredicts the abundance of massive subhaloes with respect to ROCKSTAR, SURV and our semi-analytical model. As is evident from the errorbars in the lower-right panel, this is not a manifestation of sample variance. Rather, as already discussed in connection to Figs. 3-4, this is most likely due to the issues with massive, overlapping haloes discussed in §2.2.1.
- The GIF + SURV results of Giocoli et al. (2008a) are in excellent agreement with our semi-analytical model (see also Paper I). This is particularly reassuring given that our model uses subhalo mass loss rates that have been calibrated against the same data set.

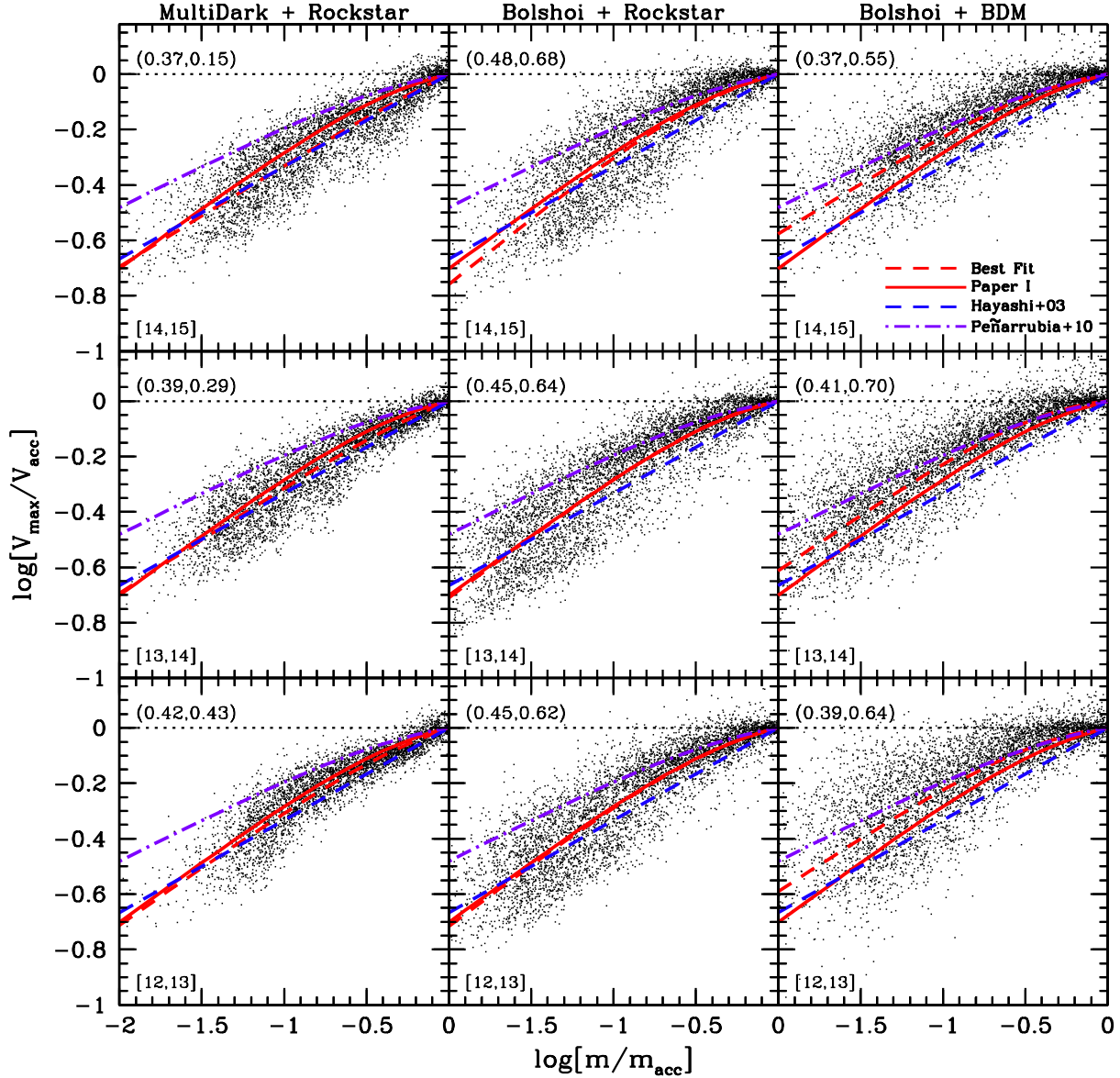


**Figure 6.** The ratio  $V_{\max}/V_{\text{acc}}$  as function of  $m/m_{\text{acc}}$  for dark matter subhaloes obtained from MultiDark+ROCKSTAR (left column), Bolshoi+ROCKSTAR (middle column) and Bolshoi+BDM (right column). Different rows correspond to different bins in host halo mass, with the range in  $\log[M/(h^{-1} M_{\odot})]$  indicated by the values in square brackets in the lower left-hand corner of each panel. In order to better sample the dependence on  $m/m_{\text{acc}}$  we plot no more than 150 subhaloes per 0.05 dex in  $\log(m/m_{\text{acc}})$ . As shown in Paper I, the  $V_{\max}/V_{\text{acc}} - m/m_{\text{acc}}$  relation is well described by Eq. (5) with  $(\eta, \mu) = (0.44, 0.60)$ , which is indicated by the solid, red line. The dashed, red lines are the best-fit relations of the form (5), fit separately to the data in each panel. The corresponding best-fit values for  $\eta$  and  $\mu$  are indicated in parenthesis in the upper left-hand corner of each panel. The blue dashed and purple dot-dashed curves are the best-fit results of Hayashi et al. (2003) and Peñarrubia et al. (2010), and are shown for comparison.

- The SHMFs obtained using SUBFIND dramatically underpredict the abundances of massive subhaloes. For cluster-sized host haloes the discrepancy with the semi-analytical model and with the SURV and ROCKSTAR results exceeds one order of magnitude for  $m/M = 0.1$ !

### 3.3 Evolution of Structural Parameters

In addition to the SHMFs,  $dN/d\log(m/M)$ , we also consider the subhalo velocity functions,  $dN/d\log(V_{\max}/V_{\text{vir}})$ , where  $V_{\text{vir}}$  is the virial velocity of the host halo. As discussed in §2.3 above, in our semi-analytical model  $V_{\max}$  for the sub-

haloes is computed using a relation between  $V_{\max}/V_{\text{acc}}$  and  $m/m_{\text{acc}}$  that is calibrated against high-resolution simulations of cluster-sized dark matter haloes from the Rhapsody project (see Paper I). Fig. 6 plots  $V_{\max}/V_{\text{acc}}$  versus  $m/m_{\text{acc}}$  for subhaloes in the MultiDark and Bolshoi simulations, obtained using either BDM or ROCKSTAR. Results are shown for three different bins in host-halo mass, as indicated in the lower left-hand corner of each panel. In order to better delineate the trends, we plot no more than 150 subhaloes per bin of 0.05 dex in  $\log(m/m_{\text{acc}})$ . The red, solid line in each panel corresponds to Eq. 5 with  $(\eta, \mu) = (0.44, 0.60)$  which is the relation that best fits the Rhapsody data and which we use

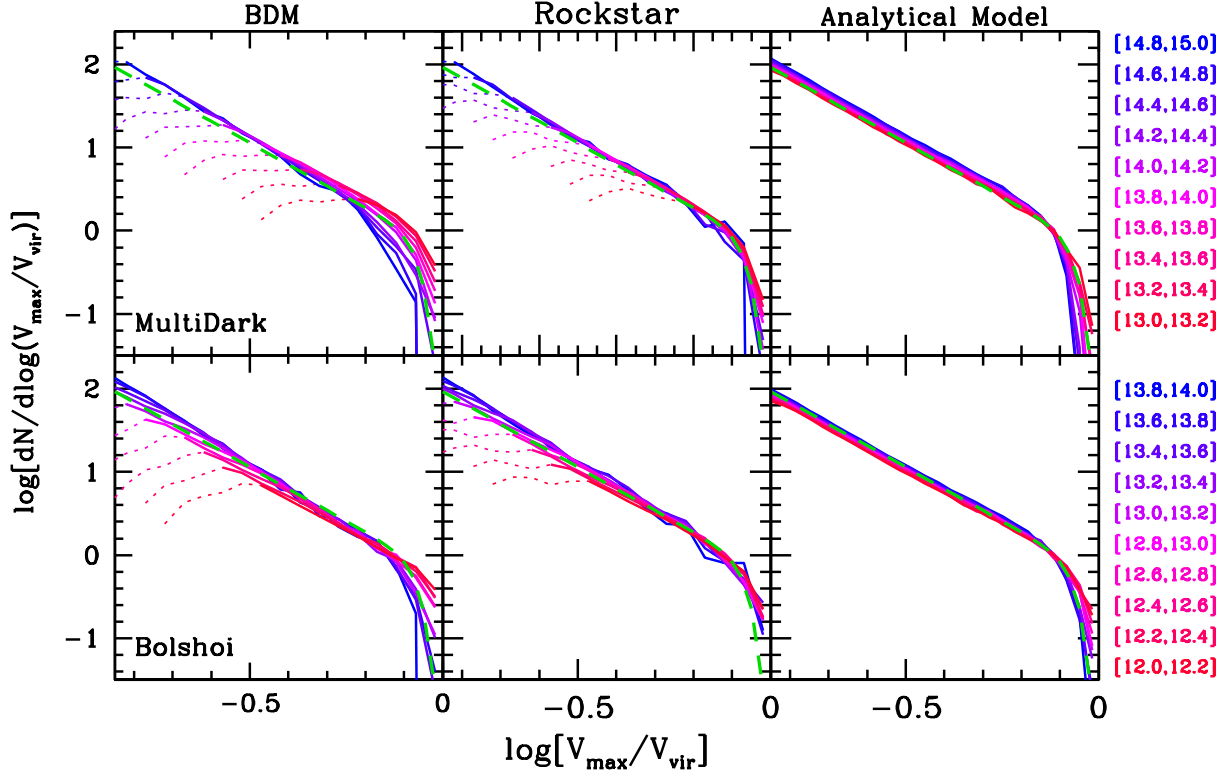


**Figure 7.** Same as Fig. 3 except here we show the subhalo velocity functions  $dN/d\log(V_{\max}/V_{\text{vir}})$ . Solid lines are the results for all subhaloes with at least 250 particles, while the dotted parts of the curves show the extensions one obtains when including subhaloes down to a limit of 50 particles per subhalo. The green, dashed curve in each panel corresponds to Eq. (7) with  $A_V = 0.57$ ,  $\beta = 2.6$ , and  $B = 7.0$ , which roughly describes the average of all SHVFs, and is shown to facilitate a comparison.

in our semi-analytical model to compute  $V_{\max}$ . The relation between  $V_{\max}/V_{\text{acc}}$  and  $m/m_{\text{acc}}$  has also been studied by Hayashi et al. (2003) and Peñarrubia et al. (2008, 2010) using high-resolution, idealized  $N$ -body simulations of individual subhaloes orbiting in a static, spherical NFW host halo. Hayashi et al. found that  $V_{\max}/V_{\text{acc}} \propto (m/m_{\text{acc}})^{1/3}$ , which is indicated by a dashed, blue line in Fig. 6, and which is in reasonable agreement with the results obtained in Paper I. Peñarrubia et al. (2010) fitted their results using the functional form of Eq. (5). Their best-fit has  $(\eta, \mu) = (0.30, 0.40)$  and is indicated as a purple dot-dashed curve in Fig. 6. Finally, we use the Levenberg-Marquardt method to fit the data in each panel with Eq. (5), treating  $\eta$  and  $\mu$  as free parameters. The best-fit values for  $\eta$  and  $\mu$  are indicated in parenthesis in the upper left-hand corner of each panel, while the red, dashed line shows the corresponding best-fit relation.

Comparing panels in different rows, there is no indication for a significant dependence on host halo mass. However, comparing results in different columns, different simulations and/or subhalo finders do seem to result in  $V_{\max}/V_{\text{acc}} - m/m_{\text{acc}}$  relations that are slightly different. Overall, in the case of ROCKSTAR, the best-fit relations are in good agreement with the results of Paper I and with the simple power-law relation of Hayashi et al. (2003). This is not entirely unexpected, given that the Rhapsody project also used ROCKSTAR to identify haloes and subhaloes. There is some indication, though, that the Bolshoi simulation reveals slightly more scatter in the  $V_{\max}/V_{\text{acc}} - m/m_{\text{acc}}$  re-

lation than the MultiDark simulation. More dramatic are the differences between the BDM and ROCKSTAR analyses of the Bolshoi simulation. The BDM results are offset to larger  $V_{\max}/V_{\text{acc}}$  at given  $m/m_{\text{acc}}$ , and display a larger scatter especially at low  $m/m_{\text{acc}}$ .

These differences emphasize that not only the abundances, but also the structural properties of dark matter subhaloes, are sensitive to the subhalo finder used. Overall, though, the best-fit relations, indicated by the dashed, red lines, are nicely bracketed by the results based on idealized simulations by Hayashi et al. (2003) and Peñarrubia et al. (2010), and in general the solid, red line, which is used in our model, is a reasonable description of the average trend. More detailed investigations are needed to investigate the origin of the differences between the various simulation results, although we suspect that they are largely due to subtleties related to how subhaloes masses are determined.

### 3.4 Subhalo Velocity Functions

The right-hand panels of Fig. 7 show the subhalo velocity functions (SHVFs),  $dN/d\log(V_{\max}/V_{\text{vir}})$ , obtained using our semi-analytical model. These correspond to the SHMFs shown in the corresponding panels in Fig. 3, and reveal a similar dependence of normalization on host halo mass, at least at the low velocity end. In particular, the model predicts that more massive host haloes have a larger abundance of subhaloes at fixed  $V_{\max}/V_{\text{vir}} \lesssim 0.6$ . At the high velocity end, though, where the velocity function cuts off exponen-

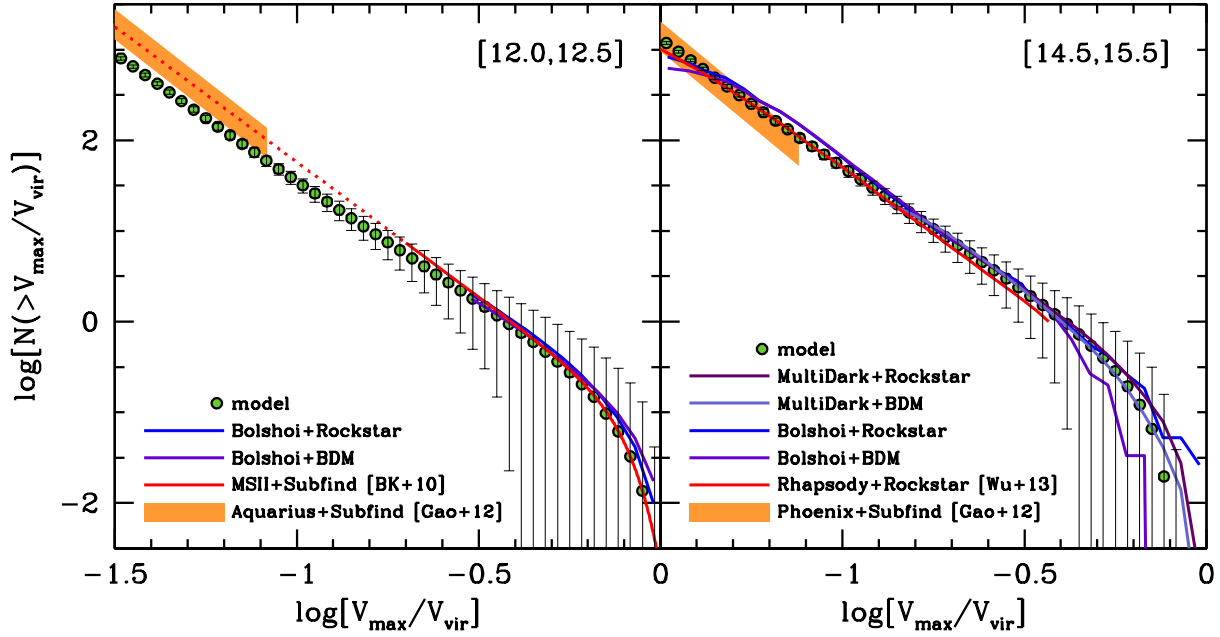


**Figure 8.** Cumulative subhalo velocity functions for host haloes with  $\log[M/(h^{-1} M_{\odot})]$  in the range  $[12.0, 12.5]$  (left-hand panel) and  $[14.5, 15.5]$  (right-hand panel). The green dots are the results obtained using our semi-analytical model, averaging over 5,000 host haloes, while the errorbars indicate the standard deviation due to halo-to-halo variance. In addition to the results from Bolshoi and MultiDark (using only subhaloes resolved with at least 250 particles), we also overplot results from ROCKSTAR for the Rhapsody simulations, and from SUBFIND for the Millennium Simulations II, the Aquarius simulations and the Phoenix simulations.

tially, this trend reverses sign. This indicates that, unlike the SHMFs, the SHVFs are not self-similar! As shown in Paper I, this is already imprinted in the unevolved SHVF (i.e., using the values of  $V_{\max}$  at accretion), and is a consequence of the concentration-mass-redshift relation of dark matter haloes, which induces a mass dependence in the ratio  $V_{\max}/V_{\text{vir}}$  of host haloes. The model SHVFs are well fit by

$$\frac{dN}{d \log(V_{\max}/V_{\text{vir}})} = A_V \left( \frac{V_{\max}}{V_{\text{vir}}} \right)^{-\beta} \exp \left[ -B (V_{\max}/V_{\text{vir}})^{15} \right]. \quad (7)$$

with slope  $\beta = 2.6$  and a normalization  $A_V$  that depends (weakly) on host halo mass. Contrary to the SHMFs, the scale parameter  $B$  now also depends on halo mass (and, as discussed in detail in Paper I, also on redshift and cosmology). The green, dashed line in each panel corresponds to Eq. (7) with  $A_V = 0.57$ ,  $\beta = 2.6$ , and  $B = 7.0$ , which roughly describes the average of all SHVFs shown.

The left and middle panels of Fig. 7 show the SHVFs obtained from the MultiDark (upper panels) and Bolshoi (lower panels) simulations using both BDM (left-hand panels) and ROCKSTAR (middle panels). The solid curves are the SHVFs obtained using only subhaloes with at least 250 particles. The dotted parts of the curves show the extensions one obtains when including subhaloes down to a limit of 50 particles per subhalo, which is the same limit as used for the SHMFs in Fig. 3. As is evident, including haloes with fewer than  $\sim 250$  particles results in SHVFs that are clearly affected by resolution effects. Boylan-Kolchin et al. (2010), in their analysis of the Millennium II simulation, argued that the minimum number of particles required to resolve haloes well enough for a reliable estimate of  $V_{\max}$  is 150. Our re-

sults, though, indicate that this limit has to be increased to  $\sim 250$ , at least for the MultiDark and Bolshoi simulations used here.

Comparing the SHVFs obtained from the simulations with those predicted by our semi-analytical model, similar trends are apparent as for the SHMFs. Simulation results and model predictions are in good agreement when it comes to the normalization and slope at the low-velocity end of the SHVFs (i.e., where  $V_{\max}/V_{\text{vir}} \lesssim 0.5$ ). However, at the massive end, where the SHVFs reveal an exponential cut-off, significant differences are apparent, albeit less pronounced than in the case of the SHMFs. As with the subhalo mass functions, the BDM results reveal a much more pronounced dependence on host halo mass compared to either the ROCKSTAR results or the predictions from our semi-analytical model. This most likely is yet another manifestation of the problem that BDM has with the treatment of massive subhaloes (see discussion in §2.2.1).

Fig. 8 compares the *cumulative* subhalo velocity functions,  $N(> V_{\max}/V_{\text{vir}})$  for two bins in host halo mass:  $\log[M/(h^{-1} M_{\odot})] \in [12.0, 12.5]$  (left-hand panel) and  $[14.5, 15.5]$  (right-hand panel). The green dots are the results obtained using our semi-analytical model, averaging over 5,000 host haloes, while the errorbars indicate the standard deviation due to halo-to-halo variance. In addition to the results from Bolshoi and MultiDark (using only subhaloes resolved with at least 250 particles), we also overplot results from ROCKSTAR for the Rhapsody simulations, and from SUBFIND for the Millennium Simulations II, the Aquarius simulations and the Phoenix simulations. The results from the Aquarius and Phoenix simulations are taken from Gao et al. (2012), who defined host haloes as spheres with a radius of  $r_{200c}$ . We have converted their results to

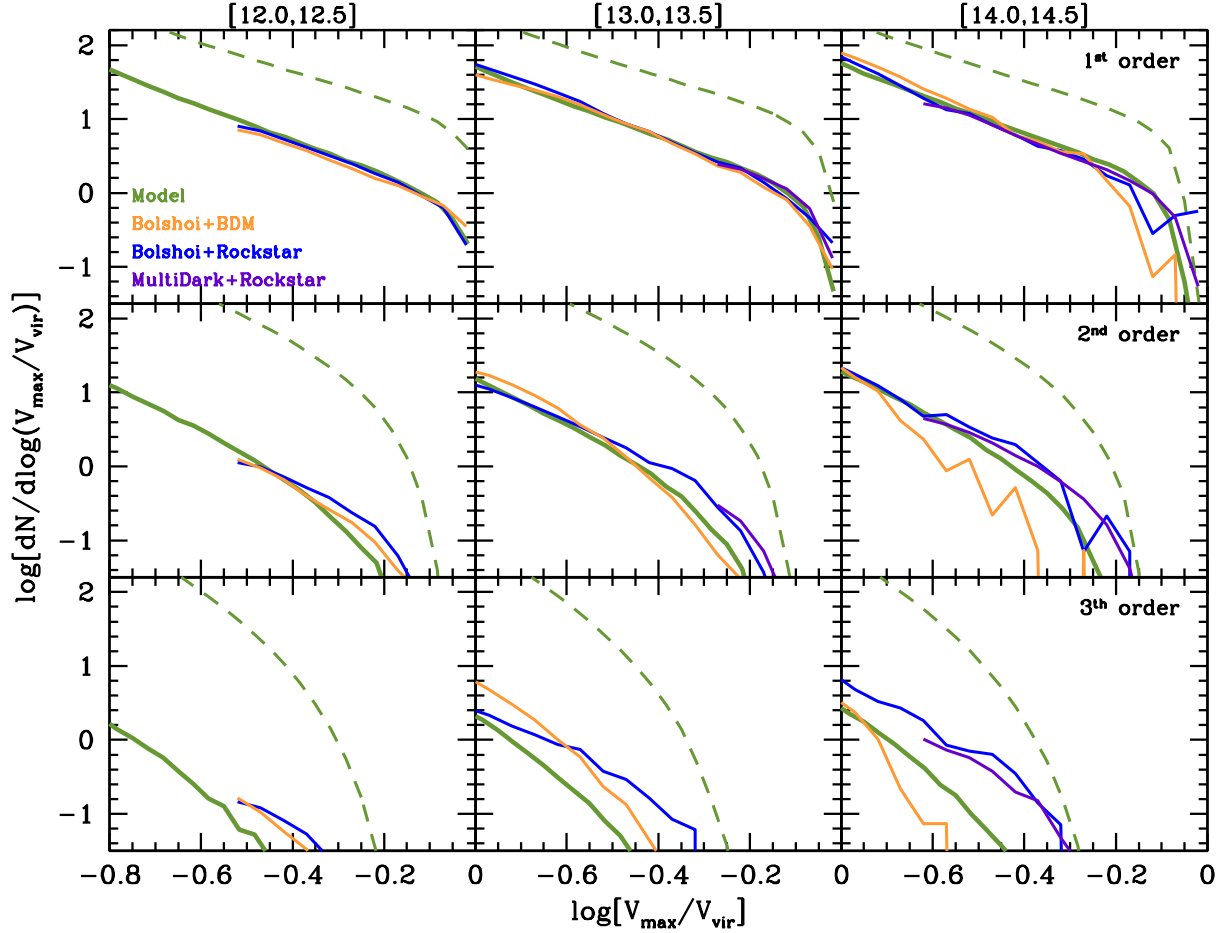


**Figure 9.** Subhalo velocity functions of first order (upper row), second order (sub-subhaloes, middle row) and third order (sub-sub-subhaloes; lower row). Results are shown for three different bins in host halo mass, as indicated by the values in square brackets at the top of each column. Solid, green lines are the model results, obtained by averaging over 5,000 host haloes. The other curves are the results obtained from the Bolshoi and MultiDark simulations, using only subhaloes with at least 250 particles, as indicated in the top-left panel. The dashed, green curves are the unevolved SHVFs, as obtained from our semi-analytical model, and are shown for comparison.

our definition of halo mass and radius. The lower boundary of the orange band shown corresponds to a conversion in which we assume that subhaloes follow the density distribution of the dark matter, while the upper boundary marks the results obtained assuming that subhaloes are homogeneously distributed within their host. These two extremes bound the true distribution of subhaloes. Overall the agreement between the various simulation results and the semi-analytical model is extremely good. In particular, the MSII + SUBFIND results from Boylan-Kolchin et al. (2010) accurately match the model predictions as well as both the ROCKSTAR and BDM results obtained from the Bolshoi simulation. This demonstrates that the dramatic discrepancies between these results in the SHMFs (cf. Fig. 5) arise from issues related to assigning masses to the subhaloes, rather than from issues related to detecting them. The maximum circular velocity probes the inner regions of dark matter haloes, and is therefore a much more robust quantity to measure in simulations than subhalo mass.

The main deviant with respect to our model predictions are the Aquarius results of Gao et al. (2012), which have a larger normalization and a significantly steeper slope. Note that the extrapolation of the MSII + SUBFIND results

by Boylan-Kolchin et al. (2010), indicated by the red, dotted curve in the left-hand panel, is in good agreement with the Aquarius results, suggesting that this is largely a SUBFIND issue. Gao et al. (2012) fitted their cumulative SHVFs with a power-law,  $N(> V_{\max}) \propto V_{\max}^{-\zeta}$ , over the range  $0.025 \leq V_{\max}/V_{200c} \leq 0.1$ , which roughly corresponds to  $0.02 \leq V_{\max}/V_{\text{vir}} \leq 0.08$ , and measured slopes of  $\zeta = 3.13$  and  $3.32$  for the Aquarius and Phoenix simulations, respectively. This is significantly steeper than our model predictions, which have  $\zeta \simeq 2.75 \pm 0.05$ <sup>¶</sup>. Unfortunately, we have not been able to find any other simulation results that can be used to investigate these discrepancies for the [12.0, 12.5] mass bin. However, in the case of the cluster-sized haloes, we can include the Rhapsody and Bolshoi simulations in the comparison. Whereas our model predictions are in excellent agreement with the Rhapsody results, they are somewhat too low around  $V_{\max}/V_{\text{vir}} \sim 0.1$  compared to the Bolshoi results. Given the level of disagreement between the various

<sup>¶</sup> We caution that, depending on the range over which it is measured, the slope of the cumulative velocity function,  $\zeta$ , can differ significantly from that of the differential SHVF,  $\beta$



simulation results, we conclude that, at this stage, there is no indication that the model predictions are incorrect. More detailed simulation results are required to further test our model prediction that the slope of the (cumulative) SHVF is significantly shallower than 3.0. We emphasize that accurate knowledge of this slope is important for various areas of astrophysics, in particular for making accurate predictions for the expected dark matter annihilation signal (e.g., Bergstrom et al. 1999; Colafrancesco, Profumo & Ullio 2006; Giocoli et al. 2008b).

### 3.5 Higher-order substructure

Thus far, all subhalo mass and velocity functions shown are for *all* subhaloes, irrespective of their order. We now shift our focus to subhaloes of different orders. In what follows we only present results for subhalo velocity functions, though results for the subhalo mass functions are qualitatively similar. Fig. 9 plots the SHVFs for subhaloes of first, second and third order (different rows) for host haloes in three different bins of host halo mass, as indicated at the top of each column. Solid green lines are the model predictions, obtained averaging over 5,000 host haloes. The dashed, green lines are the corresponding *unevolved* subhalo velocity functions (i.e., using  $V_{\text{acc}}$  rather than  $V_{\text{max}}$ ) of the same order. The evolved SHVFs are reduced with respect to the unevolved ones due to mass stripping, which reduces the subhalo's  $V_{\text{max}}$  according to Eq. (5).

Overplotted are the results obtained from the Bolshoi and MultiDark simulations. They are in superb agreement with our model predictions for the first-order subhaloes. However, very significant discrepancies are apparent for the second- and third-order subhaloes, not only between the simulation results and our model predictions, but also between the different simulation results. Whereas the ROCKSTAR results obtained from Bolshoi are in good agreement with those from MultiDark, they are very different from those obtained using BDM, especially in the more massive host haloes. These discrepancies among the simulation results make it difficult to judge the reliability of the model. In principle, there are a few oversimplifications in the model that could result in inaccuracies. First of all, in our model subhaloes can only increase their order with time. This ignores the possibility that higher-order subhaloes are stripped from their direct parent, thereby reducing their order by one. If this occurs frequently, our model will underestimate the abundance of subhaloes of a given order. Our model also ignores potential mergers among subhaloes. However, since there is no obvious reason for stripping or merging to be more frequent or relevant for higher-order subhaloes than for first-order subhaloes, and given the fact that our model is in excellent agreement with the simulation results for first-order subhaloes, we consider it unlikely that these shortcomings would have a significant impact. Rather, we believe that these discrepancies are more likely a manifestation of the subtle differences between how model and simulations treat ‘overlapping’ haloes (see §2.4 and Fig. 1).

## 4 SUMMARY

We have compared subhalo mass and velocity functions obtained from different simulations, with different subhalo finders, among each other and with predictions from our new semi-analytical model presented in Paper I. Our findings can be summarized as follows:

- We confirm the findings of Onions et al. (2012) and Knebe et al. (2013) that the subhalo mass functions obtained using different subhalo finders agree with each other at the level of  $\sim 20$  percent. However, this is only true for low-mass subhaloes with  $m/M \lesssim 0.1$ ; at the more massive end, different subhalo finders yield SHMFs that differ by more than an order of magnitude!
- Subhalo finders that identify subhaloes based purely on density in configuration space, such as SUBFIND and BDM, dramatically underpredict, by more than an order of magnitude, the abundances of massive subhaloes (with masses  $m \gtrsim M/10$ ), especially in more massive host haloes. These problems are much less severe for the subhalo velocity functions, indicating that they arise from issues related to assigning masses to the subhaloes, rather than from issues related to detecting them. The maximum circular velocity probes the inner regions of dark matter haloes, and can therefore be measured much more reliably than subhalo mass.
- Overall our model predictions are in excellent agreement with simulation results obtained using the more advanced subhalo finders ROCKSTAR and SURV. In particular, the model accurately reproduces the slope and host-mass-dependent normalization of both the subhalo mass and velocity functions. There are small discrepancies at the very massive end, but rather than reflecting an inaccuracy of the model, these arise from subtle issues having to do with the exact halo mass definitions of overlapping haloes.
- Since tidal stripping and heating impact the outskirts of subhaloes much more than their inner regions, a large reduction in mass only has a relatively mild impact on the maximum circular velocity (Hayashi et al. 2003; Peñarrubia et al. 2008, 2010). We confirm our findings from Paper I that, on average, the relation between  $V_{\text{max}}/V_{\text{acc}}$  and  $m/m_{\text{acc}}$  is well described by Eq. (5) with  $(\eta, \mu) = (0.44, 0.60)$ , which is roughly bracketed by the relations obtained by Hayashi et al. (2003) and Peñarrubia et al. (2010) using idealized  $N$ -body simulations. However, there are small but noticeable differences in the best-fit values of  $\eta$  and  $\mu$  for different subhalo finders, indicating that not only the abundances, but also the structural properties of dark matter subhaloes, are sensitive to the subhalo finder used.
- The mass and velocity functions obtained from the Bolshoi and MultiDark simulations confirm our finding from Paper I that the power-law slopes of  $dN/d\log(m/M)$  and  $dN/d\log(V_{\text{max}}/V_{\text{vir}})$  are with 0.82 and 2.6, respectively, significantly shallower than what has been claimed in several studies in the literature. In particular, studies based on SUBFIND by Boylan-Kolchin et al. (2010) and Gao et al. (2012) have yielded slopes that are significantly steeper. Given the excellent agreement between our model predictions and the ROCKSTAR, BDM and SURV results, we believe that this discrepancy reflects a problem with SUBFIND. We emphasize that accurate knowledge of the power-law slope of the subhalo mass and velocity functions is important for calculating the ‘boost’ factor for dark matter annihilation.



tion due to substructure, as this requires extrapolation of  $dN/d\log(m/M)$  down to the dark matter Jeans mass.

- Comparing the velocity functions for subhaloes of different order, we find that our model is in excellent agreement with the Bolshoi and MultiDark results for first-order subhaloes. This agreement, however, rapidly deteriorates with increasing order; not only between model and simulations, but also among the simulation results themselves. We speculate that these discrepancies are mainly a manifestation of subtle issues having to do with how different subhalo finders treat overlap among haloes and subhaloes. More detailed studies are required to investigate these issues further, and to provide a more reliable testbed for our model predictions.

## ACKNOWLEDGMENTS

We are grateful to the people responsible for the Bolshoi and MultiDark simulations for making their halo catalogs publicly available, and to the following individuals for their advice and assistance: Peter Behroozi, Mike Boylan-Kolchin, Carlo Giocoli, Andrew Hearin, Anatoly Klypin, Alexander Knebe, Surhud More, Nikhil Padmanabhan, Tomomi Sunayama, and Bepi Tormen.

## REFERENCES

- Angulo R.E., Lacey C.G., Baugh C.M., Frenk C.S., 2009, MNRAS, 399, 983
- Behroozi P. S., Wechsler R. H., Wu H.-Y., 2013a, ApJ, 762, 109
- Behroozi P. S., Wechsler R. H., Wu H.-Y., Busha M.T., Klypin A.A., Primack J.R., 2013b, ApJ, 763, 18
- Bergstrom L., Edsjo J., Gondolo P., Ullio P., 1999, Phys.Rev.D., 59, 043506
- Boylan-Kolchin M., Springel V., White S.D.M., Jenkins A., Lemson G., 2009, MNRAS, 398, 1150
- Boylan-Kolchin M., Springel V., White S.D.M., Jenkins A., 2010, MNRAS, 406, 896
- Bryan G., Norman M., 1998, ApJ, 495, 80
- Busha M.T., Wechsler R.H., Behroozi P.S., Gerke B.F., Klypin A.A., Primack J.R., 2011, ApJ, 743, 117
- Colafrancesco S., Profumo S., Ullio P., 2006, A&A, 455, 21
- De Lucia G., et al., 2004, MNRAS, 348, 333
- Diemand J., Moore B., Stadel J., 2004, MNRAS, 352, 535
- Diemand J., Kuhlen M., Madau P., 2006, ApJ, 649, 1
- Diemand J., Kuhlen M., Madau P., 2007, ApJ, 667, 859
- Gao L., De Lucia G., White S.D.M., Jenkins A., 2004, MNRAS, 352, 1
- Gao L., Frenk C.S., Boylan-Kolchin M., Jenkins A., Springel V., White S.D.M., 2011, MNRAS, 410, 2309
- Gao L., Navarro J.F., Frenk C.S., Jenkins A., Springel V., White S.D.M., 2012, MNRAS, 425, 2169
- Ghigna S., Moore B., Governato F., Lake G., Quinn T., Stadel J., 2000, ApJ, 544, 616
- Gill S.P.D., Knebe A., Gibson B.K., 2004a, MNRAS, 351, 399
- Gill S.P.D., Knebe A., Gibson B.K., Dopita M.A., 2004b, MNRAS, 351, 410
- Giocoli C., Tormen G., van den Bosch F.C., 2008a, MNRAS, 386, 2135
- Giocoli C., Pieri L., Tormen G., 2008b, MNRAS, 387, 689
- Giocoli C., Tormen G., Sheth R.K., van den Bosch F.C., 2010, MNRAS, 404, 502
- Giocoli C., Tormen G., Sheth R. K., 2012, MNRAS, 422, 185
- Han J., Jing Y.P., Wang H., Wang W., 2012, MNRAS, 427, 2437
- Hayashi E., Navarro J.F., Taylor J.E., Stadel J., Quinn T., 2003, ApJ, 584, 541
- Helmi A., White S.D.M., Springel V., 2002, Phys. Rev. D., 66, 063502
- Jiang F., van den Bosch F.C., 2014a, MNRAS, in press (arXiv:1311.5225)
- Jiang F., van den Bosch F.C., 2014b, MNRAS, submitted (paper I)
- Klypin A., Holtzman J., 1997, preprint (arXiv:astro-ph/9712217)
- Klypin A., Kravtsov A.V., Valenzuela O., Prada F., 1999, ApJ, 522, 82
- Klypin A.A., Trujillo-Gomez S., Primack J.R., 2011, ApJ, 740, 102
- Knebe A., et al., 2011, MNRAS, 415, 2293
- Knebe A., et al., 2013, MNRAS, 435, 1618
- Knollmann S.R., Knebe A., 2009, ApJS, 182, 608
- Kravtsov A.V., Berlind A.A., Wechsler R.H., Klypin A.A., Gottlöber S., Allgood B., Primack J.R., 2004, ApJ, 609, 35
- Ludlow A.D., et al., 2013, MNRAS, 432, 1103
- Maccio A.V., Dutton A.A., van den Bosch F.C., 2008, MNRAS, 391, 1940
- Maciejewski M., Colomby S., Springel V., Alard C., Bouchet F.R., 2005, MNRAS, 396, 1329
- Moore B., Ghigna S., Governato F., Lake G., Quinn T., Stadel J., Tozzi P., 1999, ApJ, 524, L19
- Muldrew S.I., Pearce F.R., Power C., 2011, MNRAS, 410, 2617
- Navarro J.F., Frenk C.S., White S.D.M., 1997, ApJ, 490, 493
- Neyrinck M.C., Gnedin N.Y., Hamilton A.J.S., 2005, MNRAS, 356, 1222
- Onions J., et al., 2012, MNRAS, 423, 1200
- Parkinson H., Cole S., Helly J., 2008, MNRAS, 383, 557
- Peñarrubia J., Navarro J.F., McConnachie A.W., 2008, ApJ 673, 226
- Peñarrubia J., Benson A.J., Walker M.G., Gilmore G., McConnachie A.W., Mayer L., 2010, MNRAS, 406, 1290
- Prada F., Klypin A.A., Cuesta A.J., Betancort-Rijo J.E., Primack J., 2012, MNRAS, 423, 3018
- Reed D., Governato F., Quinn T., Gardner J., Stadel J., Lake G., 2005, MNRAS, 359, 1537
- Riebe K., et al., 2013, Astron. Nachrichten, 334, 691
- Shaw L.D., Weller J., Ostriker J.P., Bode P., 2006, ApJ, 646, 815
- Shaw L.D., Weller J., Ostriker J.P., Bode P., 2007, ApJ, 659, 1082
- Springel V., White S.D.M., Tormen G., Kauffmann G., 2001, MNRAS, 328, 726
- Springel V., et al., 2005, Nature, 435, 629
- Springel V., et al., 2008, MNRAS, 391, 1685
- Somerville R.S., Kolatt T.S., 1999, MNRAS, 305, 1
- Stadel J.G., 2001, PhD, Univ. of Washington
- Stoehr F., White S.D.M., Tormen G., Springel V., 2002, MNRAS, 335, 762
- Tormen G., 1997, MNRAS, 290, 411
- Tormen G., Diaferio A., Syer D., 1998, MNRAS, 299, 728
- Tormen G., Moscardini L., Yoshida N., 2004, MNRAS, 350, 1397
- van den Bosch F.C., Tormen G., Giocoli C., 2005, MNRAS, 359, 1029
- Vegetti S., Koopmans L.V.E., Bolton A., Treu T., Gavazzi R., 2010, MNRAS, 408, 1969
- Vegetti S., Lagattuta D.J., McKean J.P., Auger M.W., Fassnacht C.D., Koopmans L.V.E., 2012, Nature, 481, 341
- Wechsler R.H., Bullock J.S., Primack J.R., Kravtsov A.V., Dekel A., 2002, ApJ, 568, 52
- Weinberg D.H., Colomby S., Davé R., Katz N., 2008, ApJ, 678, 6
- Wu H.-Y., Hahn O., Wechsler R.H., Behroozi P.S., Mao Y.-Y., 2013, ApJ, 767, 23
- Zhao D.H., Jing Y.P., Mo H.J., Börner G., 2009, ApJ, 707, 354